Mechatronics 24 (2014) 12–22

Contents lists available at ScienceDirect

Mechatronics

journal homepage: www.elsevier.com/locate/mechatronics

Hysteresis modeling and position control of tendon-sheath mechanism in flexible endoscopic systems

T.N. Do [a], T. Tjahjowidodo [a,*], M.W.S. Lau [b], T. Yamamoto [a], S.J. Phee [a]

[a] School of Mechanical and Aerospace Engineering, Nanyang Technological University, 50 Nanyang Avenue, Singapore 639798, Singapore
[b] School of Mechanical and Systems Engineering, Newcastle University, UK

ARTICLE INFO

Article history:
Received 7 June 2013
Accepted 15 November 2013
Available online 6 December 2013

Keywords:
Tendon-sheath mechanism
Surgical robot
Backlash hysteresis
Modeling
Feedforward
Endoscopic systems

ABSTRACT

Tendon-sheath mechanism has "revolutionized" the use of flexible endoscopic systems, by its many advantages of high maneuverability, lightweight, low cost, and simple design. However, nonlinear phenomena such as friction and backlash hysteresis present major challenges for motion control of the tool tips. This paper introduces a new mathematical model and a control scheme for the tendon-sheath mechanism for use in endoscopic systems. The asymmetric backlash hysteresis model that characterizes the transmission phenomena of the tendon-sheath mechanism in the loading and unloading phases is presented and discussed. An efficient parameter identification method is used to estimate the model parameters. Comparisons between the proposed model and experimental data validate the adoption of this new approach. A feedforward compensation method based on the asymmetric backlash hysteresis model is proposed and explored. The proposed model and control scheme are validated by experimental studies using a suitable experimental setup. The results show that the proposed model and the control scheme can improve the accuracy of tendon-sheath mechanism without using any output feedback and can be easily implemented in surgical robots using tendon-sheath mechanism as the main mode of transmission.

1. Introduction

Flexible endoscopic systems are being used in many diagnostic procedures such as colonoscopies, gastroscopies, and surgical tasks. One of the common transmission modes in these systems is the tendon-sheath mechanism. It offers some advantages as it can operate in small working areas, allow for drastic reduction of size, lightweight, capability of transmitting high load, and high maneuverability.

The mechanical structure of a tendon-sheath mechanism is illustrated in Fig. 1(a). A tendon-sheath mechanism consists of a hollow helical coil wire acting as a sheath and a cable slides inside the sheath acting as a tendon. When the tendon is pulled at one end, it slides inside the sheath and transmits the motion and force to the other side of the sheath. In a flexible endoscopic system, the tendon-sheath mechanisms are routed along an endoscope, which can access to a potential surgical sites via natural orifices of patient [1]. They are connected to the slave manipulator to actuate joints and perform suitable surgical tasks inside the human's body (Fig. 1(b)). The slave manipulator, which has two robotic arms, can undertake the tasks of gripping and cutting the target tissues. In order to handle various tasks during the operation, each robotic arm has its own degrees of freedom (DOFs). These DOFs are controlled by the tendon-sheath mechanisms.

The tendon-sheath mechanism has been used in many surgical systems, such as telemanipulated system for transluminal surgery [2], ViaCath robotic system [3], MASTER robot [1], and Laprotek surgical system [4]. When the output information like position and force at the slave manipulator are not available for feedback due to sterilization problems and its size, a camera at the end of endoscope is used to provide visual feedback to the surgeons. Although the tendon-sheath mechanism has many advantages, the performances are still limited by its nonlinear friction and backlash hysteresis phenomena. These nonlinearities pose some difficulties in predicting the force at the tool tips and challenges in controlling the precise motion of the system. Moreover, traditional sensors cannot be mounted on the tool tips to provide the necessary feedbacks because of practical limitations (sterilization and size). Therefore, the controller strategy of such system is open loop with no feedbacks.

Recently, several researchers have addressed the nonlinear characteristics of the tendon-sheath mechanism with various analytical models of friction and motion, in which the sheath curvature and static friction model are the main concerns. Some preliminary analyses have been proposed by Kaneko et al. [5,6]. Despite the absence of the controller strategy in the system, the

* Corresponding author. Tel.: +65 6790 4952; fax: +65 6792 4062.
E-mail address: ttegoeh@ntu.edu.sg (T. Tjahjowidodo).

0957-4158/$ - see front matter © 2013 Elsevier Ltd. All rights reserved.
http://dx.doi.org/10.1016/j.mechatronics.2013.11.003

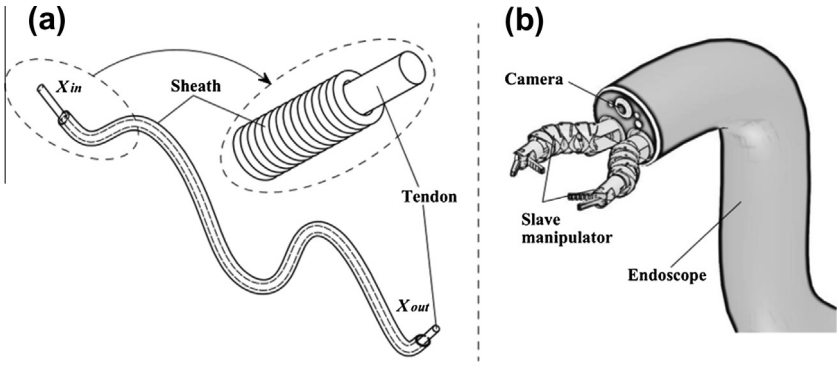

Fig. 1. (a) Tendon-sheath mechanism and (b) flexible endoscope with slave manipulator.

authors successfully introduced the transmission of tendon tension in terms of lumped mass model parameter with Coulomb friction model. Palli et al. [7,8] modeled the tendon-sheath mechanism by taking into consideration a dynamic friction model (Dahl [9]) in combination with the lumped mass model parameters. However, it is shown that this approach is rather complex when more tendon elements are considered and discontinuity problem exists when the tendon-sheath mechanism operates near zero velocity. In addition, no control schemes of motion are introduced to compensate for the errors. The same approaches were also carried out by Tian et al. and Low et al. [10,11] where the assumption of the same initial pretension for each of tendon elements was considered. Agrawal et al. [12,13] first used a set of partial differential equations to model the tendon sheath by considering a number of tendon segments. However, with this approach it is difficult to determine whether the tendon segments are moving or stable while the discontinuous problems in areas near zero velocity still exist. Later, they utilized a smooth hysteresis inverse to reduce the effect of backlash in the motion of Laprotek robotic arm [14,15]. Kesner et al. [16,17] implemented a compensation method to improve the tracking performances for a robotic catheter system, where the backlash profile was based on the width of the hysteresis curves. These approaches considered the control problems under the assumption of the presence of a feedback from the tool tips. In practice, this assumption is not valid for most surgical robots in use. Moreover, their proposed schemes, based on the inversion of backlash hysteresis models, lead to a computational higher cost for the compensator and are still limited by discontinuous problems arising from the approach in modelling. In addition, the paper does not discuss control problems in cases of multiple frequencies and variations of amplitude in the input signals. To overcome these shortcomings, backlash hysteresis models and control schemes with higher accuracy and degree of smoothness, and ease of implementation are desired. Several mathematical models of backlash hysteresis including the Duhem model, Preisach model, Prandtl–Ishlinskii (PI) model were introduced and discussed in Macki et al. [18] and Hassani et al. [19]. The PI and Preisach are modeled by the sum of many elementary hysteresis namely hysterons, which increases the complexity in implementation and computation if a high number of elements are considered. The Bouc–Wen model [20], which is a special form of the Duhem model [21], can provide an accurate approximation of backlash-like hysteresis curves and capture a wide range of hysteresis phenomena. This model is able to control the amplitudes and shapes of the hysteresis loops as well as the smoothness of transition phases from positive velocity to negative velocity using a flexible set of parameters.

In this paper, we propose a new approach to model and identify the nonlinear backlash hysteresis phenomena of a tendon-sheath mechanism under various input signals. Compared to the existing approaches, the proposed model allows for the capture of backlash hysteresis nonlinearities regardless to the curvature and sheath angles. To compensate for the backlash hysteresis phenomena, a feedforward control scheme based on the inverse multiplicative method is proposed and explored. This method is used in many applications of piezoelectric actuations, as it does not require any complex inversion of backlash hysteresis model and allows for easy implementations [21–23]. In order to validate the effectiveness of the approach, a suitable experimental setup is established.

In Section 2, the experimental work will be presented. Section 3 introduces a review of current backlash hysteresis models and a new asymmetric backlash hysteresis model for the tendon-sheath mechanism. Section 4 introduced the identification method of model parameters and comparisons between experimental results and the proposed model. The control scheme with asymmetric backlash hysteresis model-based feedforward compensation will be expressed in Section 5. Section 6 will show discussions of all approaches in this paper. Finally, the conclusion is drawn in Section 7.

2. Experimental setup and preliminary results

A dedicated experimental setup, shown in Fig. 2, is established to investigate the backlash hysteresis nonlinearity in a tendon-sheath mechanism. The tendon-sheath mechanism, from Asahi Intecc Co., of 1 m length is used. It consists of a Teflon coated wire tendon with a specification of WR7 $\times$ 7D0.27 mm and a round-wire coil sheath with an inner diameter of 0.36 mm and outer diameter of 0.8 mm. A Faulhaber 2642W024CR DC motor is installed at the proximal end to drive the tendon system. In order to measure the input and output motion at two ends of the tendon-sheath mechanism, two high-resolution encoders E6D-CWZ1E 3600P/R 0.5 M from Omron are used. One is connected to the DC motor at the proximal end to measure the motion input (x_{in}) while the other is placed at the distal end to measure the motion output (x_{out}). At the proximal end, the tendon-sheath is fixed to a pulley, and at the distal side, it is attached to a spring, which provides a resisting or a tensioning force.

During the experiment, an initial pretension force is applied to the tendon to prevent it from slacking and the total curve angles of the sheath configuration are maintained. The feedback signals are decoded using the dSPACE real time system DS1104. When the tendon is pulled at the input side by the DC motor, the tension in the tendon will increase in response to resistance force of the spring as it is transmitted to the output side. When the DC motor reverses the direction of the motion, again, due to resistance force of the spring, the tendon is pulled back towards the distal end.

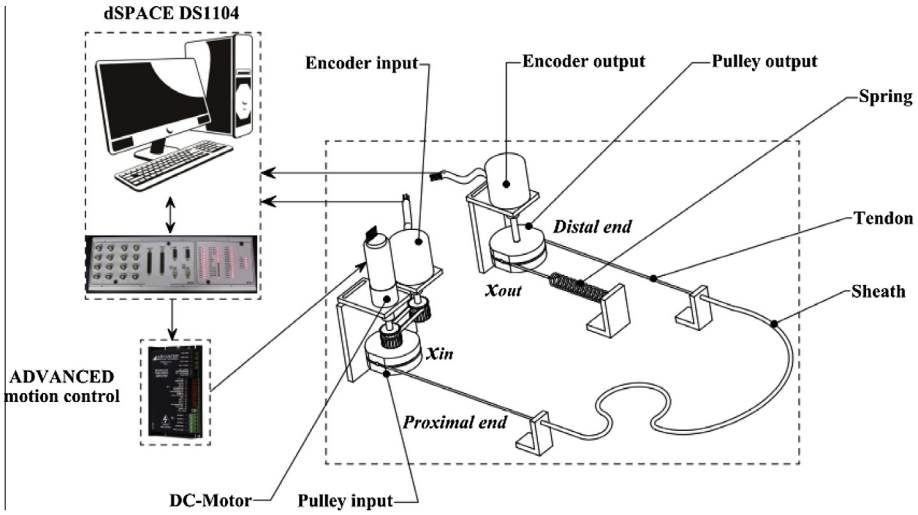

(a) Schematic setup of experimental work

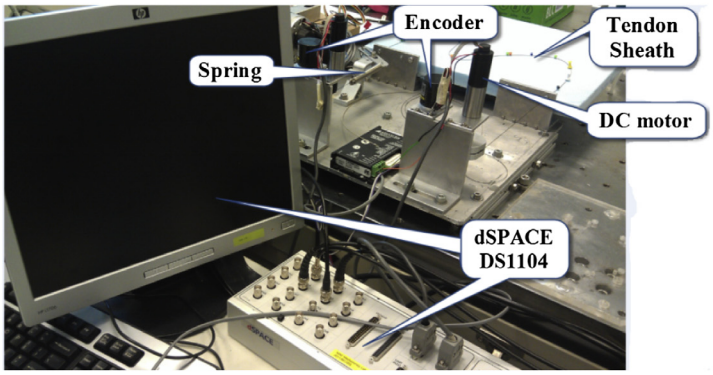

(b) Photograph of experiment

Fig. 2. Experimental setup.

In the experiment, MATLAB Simulink and the DS1104 controller board are used to generate real-time codes for system. In this paper, various input excitations will be applied to investigate the nonlinearities of backlash hysteresis phenomena in the tendon-sheath mechanism.

For position control purpose, a tendon sheath mechanism can be viewed as an element with an input displacement $x_{in}(t)$ and output displacement $x_{out}(t)$ as shown in Fig. 2(a). In the study, the system is excited using periodic and non-periodic signals. The upper panel of Fig. 3 shows the experimental results for a 0.2 Hz sinusoidal excitation with amplitude of 55°; the left panel depicts the time history of the input and output displacements and the right panel presents the relation between the input and output displacements. Similarly, the middle panel of Fig. 3 shows the result for a dual frequency sinusoidal signal of frequencies of 0.2 Hz and 0.5 Hz and amplitudes of 28°. The lower panel of Fig. 3 presents the results for a non-periodic motion with two fundamental frequencies of 0.25 Hz and $0.25\sqrt{3}$ Hz with amplitude of 28°. From the experimental results shown in Fig. 3, it can be observed that the backlash hysteresis nonlinearity in the tendon-sheath mechanism follows an asymmetric profile for both positive and negative velocity, where the width of the hysteresis loops is bigger at the upper reversal point compared to that at the lower one.

The upper panels of Fig. 4 show the experimental results for the two different configurations of the sheath shapes, i.e. Shape 01 and Shape 02 as shown in the lower panels of Fig. 4, respectively. It is observed that the backlash hysteresis profiles are not affected by the configuration of the tendon-sheath mechanism as long as the accumulated curve angles remains invariant. This observation is validated by using many experiments. However, for illustrative purpose only we depict two of the results as shown in the figure. In this case, the accumulated curve angles are maintained at 540°. This implicitly means that if the accumulated curve angle is maintained, the sheath can be flexibly configured, and the backlash hysteresis profiles are not affected.

3. Nonlinear backlash hysteresis model for tendon-sheath mechanism

For the tendon-sheath mechanism, the nonlinearities between the input displacement and the output displacement follow an approximate asymmetry of backlash hysteresis profile. Tao et al. [24] described an asymmetric backlash model by:

$$\dot{x}_{out}(t) = \begin{cases} c_1\dot{x}_{in}(t) & \text{if } \dot{x}_{in}(t) > 0 \text{ and } x_{out}(t) = c_1(x_{in}(t) - B_1) \\ c_2\dot{x}_{in}(t) & \text{if } \dot{x}_{in}(t) < 0 \text{ and } x_{out}(t) = c_2(x_{in}(t) + B_2) \\ 0 & \text{otherwise} \end{cases} \quad (1)$$

where $c_1 > 0$, $c_2 > 0$ are backlash slopes; $B_1 > 0$, $B_2 > 0$ are the width of backlash; $x_{out}(t)$ and $\dot{x}_{out}(t)$, $x_{in}(t)$ and $\dot{x}_{in}(t)$ are displacement and relative velocity at the output and input sides, respectively.

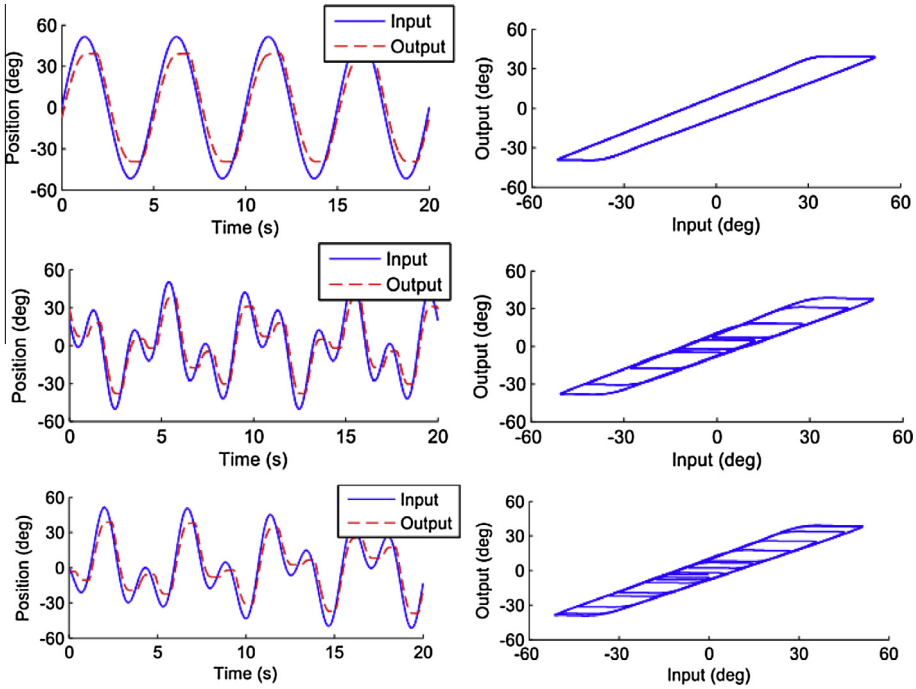

Fig. 3. Experimental results for different input signals (the unit for displacement is expressed in degree); (Upper panel) 0.2 Hz sinusoidal excitation and amplitude of 55°; (Middle panel) a dual frequency sinusoidal excitation with frequencies of 0.2 Hz and 0.5 Hz and amplitudes of 28°; (Lower panel) non-periodic input signal with two fundamental frequencies of 0.25 Hz and $0.25\sqrt{3}$ Hz with amplitude of 28°.

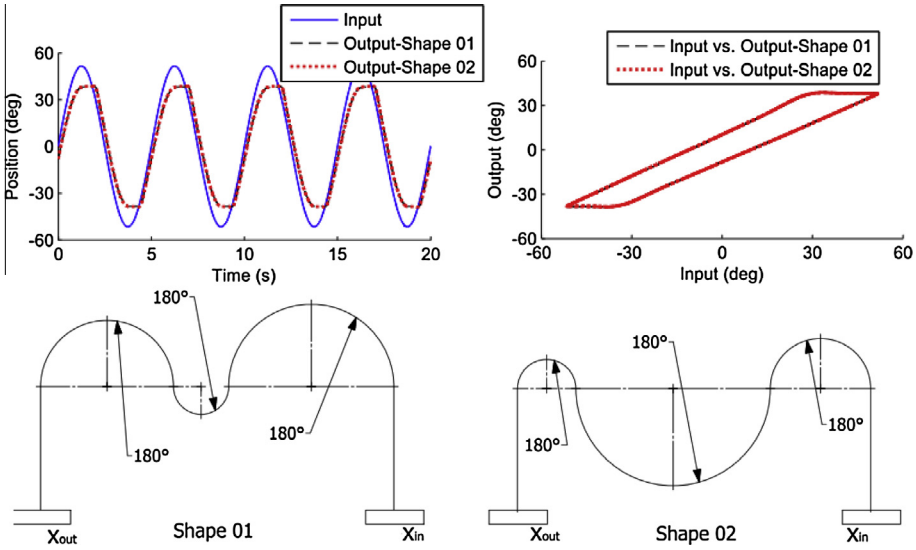

Fig. 4. Experimental results for different configurations with the same accumulated curve angles (the unit for displacement is expressed in degree); (Upper left panel) Time history of input signal; (Upper right panel) input vs. output; (Lower left panel) Shape 01; (Lower right panel) Shape 02.

The model given in Eq. (1) is discontinuous and needs complex nonlinear algorithms to control the motion of the system [25,26]. Although the Preisach and Prandtl–Ishlinskii models [18,27,28] can capture the backlash hysteresis as in the case of the tendon sheath, a large number of model parameters is required if many hysteresis elements are taken into consideration. In this paper, a model of the continuous backlash hysteresis that is appropriate for control purposes is introduced. The proposed model allows for the capture of asymmetric backlash hysteresis in the tendon-sheath mechanism and it is continuous in time. It is constructed based on several assumptions such as fixed initial pretension and fixed accumulated curve angles. Before introducing the asymmetric backlash hysteresis model for the tendon-sheath mechanism, a brief review of the current Bouc–Wen models is introduced in the next two sections.

3.1. Symmetric hysteresis Bouc–Wen model

The Bouc–Wen model of hysteresis has been used in many applications because of its ability to describe a wide range of hysteresis behavior. It uses an internal state $\zeta(t)$ and a first order differential equation [29]. Consider a map $x(t) \mapsto \Phi(x)(t)$; the symmetric Bouc–Wen model can be written as:

$$\Phi(x)(t) = \alpha_x x(t) + \alpha_\zeta \zeta(t) \tag{2}$$

$$\dot{\zeta}(t) = A\dot{x}(t) - \beta|\dot{x}(t)||\zeta(t)|^{n-1}\zeta(t) - \gamma\dot{x}(t)|\zeta(t)|^{n} \quad (3)$$

where $\Phi(x)(t) = x_{out}(t)$ is the displacement output of hysteresis system; $x(t) = x_{in}(t)$ is the displacement input. The internal state $\zeta(t)$ is the solution of the differential Eq. (3) and the dot at the top of variables represents the first derivative of the internal state with respect to time. The dimensionless parameters A, β, γ, n control the shape and size of the hysteresis loops; α_x, α_ζ are scale factors that represent the ratio of output hysteresis to the input displacement and internal state respectively. In order to use the symmetric Bouc–Wen model given by Eqs. (2) and (3), a set of six parameters has to be identified.

3.2. Generalized asymmetric Bouc–Wen model of hysteresis

The Bouc–Wen model given in Eqs. (2) and (3) cannot describe the asymmetric loops in the loading and unloading phases of the hysteresis systems. To deal with such problem, Song et al. [30] proposed a model that is able to represent a wide class of asymmetric hysteresis loops and to flexibly control the hysteresis shape. A shape control function $\Psi(x(t), \dot{x}(t), \zeta(t))$ was introduced in the model parameter. The generalized Bouc–Wen model with highly asymmetric hysteresis is expressed as follow:

$$\Phi_{Asym}(x)(t) = \alpha_x x(t) + \alpha_\zeta \zeta(t) \quad (4)$$

$$\dot{\zeta}(t) = A\dot{x}(t) - \Psi(x(t), \dot{x}(t), \zeta(t)) \quad (5)$$

$$\Psi(x(t), \dot{x}(t), \zeta(t)) = \dot{x}(t)|\zeta(t)|^{n}\Xi(x(t), \dot{x}(t), \zeta(t)) \quad (6)$$

The function $\Xi(x(t), \dot{x}(t), \zeta(t)) = \beta\Theta^T$ is combined by two vectors β and Θ:

$$\beta = [\beta_1\beta_2\beta_3\beta_4\beta_5\beta_6]$$

$$\Theta = [\mathrm{sgn}(\dot{x}\zeta)\mathrm{sgn}(\dot{x}x)sgn(x\zeta)\mathrm{sgn}(\dot{x})\mathrm{sgn}(\zeta)\mathrm{sgn}(x)]$$

where $\beta_1, \ldots, \beta_6$ are fixed parameters that control the shapes of hysteresis loop for six phases. The dimensionless parameters A and n control the scale and sharpness of the hysteresis loops; α_x, α_ζ are scale factors that represent the ratio of output hysteresis to input displacement and internal state respectively; the dot at the top of variables represents for the first derivative of internal state with respect to time. The signum function is defined by

$$\mathrm{sgn}\,(z) = \begin{cases} 1 & \text{if } z > 0 \\ 0 & \text{if } z = 0 \\ -1 & \text{if } z < 0 \end{cases}.$$

As in the symmetric Bouc–Wen model, $\Phi_{Asym}(x)(t) = x_{out}(t)$ and $x(t) = x_{in}(t)$.

To capture the asymmetric hysteresis in a system using the model given by Eqs. (4)–(6), a set of ten parameters β_1, β_2, β_3, β_4, β_5, β_6, A, n, α_x, α_ζ are to be identified.

3.3. Shortcomings of symmetric and generalized asymmetric Bouc–Wen model of hysteresis

The backlash hysteresis nonlinearity is modeled using a symmetric Bouc–Wen model given by Eqs. (2) and (3). Six parameters are optimized simultaneously using Genetic Algorithm (GA) by prescribing them as individual chromosomes in the optimization algorithm. This results in optimized parameters $\alpha_x = 0.9225$, $\alpha_\zeta = 0.6576$, $A = -1.495$, $\beta = 4.206$, $n = 1.0217$, $\gamma = 2.272$. The experimental results using this model with an input signal of sinusoidal $x(t) = x_{in}(t)$ are shown in the upper panel of Fig. 3. The backlash hysteresis loops of this Bouc–Wen model are symmetric for both loading and unloading phases. As shown in the left panel of Fig. 5, the slopes for loading and unloading phases are the same. However, experimental data obtained for the tendon sheath show that the actual curves, shown in the upper panel of Fig. 3, are asymmetric for both phases – the slopes for loading phase and unloading phase are different. Therefore, a symmetric Bouc–Wen model is not able to capture the asymmetric backlash hysteresis in the tendon sheath; it shows an increase in the errors as well as degradation in the system performances. With ten optimized parameters, i.e. $\alpha_x = 0.922$, $\alpha_\zeta = 0.4033$, $A = -1.9542$, $n = 2.024$, $\beta_1 = 14.3384$, $\beta_2 = -1.2423$, $\beta_3 = -3.0037$, $\beta_4 = -2.4624$, $\beta_5 = 0.2032$, $\beta_6 = 3.1268$, the generalized asymmetric Bouc–Wen model proposed by Song et al. [30] is able to capture the asymmetric backlash hysteresis of tendon sheath as shown in the right panel of Fig. 5. However, it requires ten parameters to model the nonlinearities. This leads to more computation and complex identification process to derive an exact set of model parameters.

3.4. A new model for asymmetric backlash-like hysteresis

An asymmetric backlash hysteresis model is introduced in this section. To model the asymmetric nonlinearity for the tendon sheath mechanism, a modification of the generalized asymmetric Bouc–Wen model with fewer numbers of parameters is required. We propose to substitute the hysteresis shape function $\Psi(x(t), \dot{x}(t), \zeta(t))$ in Eqs. (5) and (6), by a new function as presented in Eq. (7).

$$\begin{cases} \Psi(x(t), \dot{x}(t), \zeta(t)) = -\vartheta|\dot{x}(t)|\zeta(t) + \delta|\dot{x}(t)| \\ \Xi(x(t), \dot{x}(t), \zeta(t)) = \vartheta\mathrm{sgn}(\zeta(t)) \end{cases} \quad (7)$$

The output backlash hysteresis given by Eqs. (3) and (4) uses constant parameters α_x, α_ζ. In our proposed model, the parameter α_x will be established as the function of relative velocity $\dot{x}(t)$ to capture the asymmetric slopes for loading and unloading phases. To simplify the approach, the scale factor α_ζ is set as a value of one and it does not affect the model properties. The asymmetric backlash hysteresis model can be expressed by:

$$\dot{\zeta}(t) = A\dot{x}(t) - \vartheta|\dot{x}(t)|\zeta(t) + \delta|\dot{x}(t)| \quad (8)$$

$$\begin{cases} \Phi_{Asym}(x)(t) = \alpha_x(\dot{x}(t))x(t) + \zeta(t) \\ \alpha_x(\dot{x}(t)) = \frac{\alpha_1 e^{2\dot{x}(t)} + \alpha_2}{e^{2\dot{x}(t)} + 1} \end{cases} \quad (9)$$

The hyperbolic tangent is defined by $\tanh(\dot{x}(t) = \frac{e^{\dot{x}(t)} - e^{-\dot{x}(t)}}{e^{\dot{x}(t)} + e^{-\dot{x}(t)}}$; the function $\alpha_x(\dot{x}(t))$ is expressed by: $\alpha_x(\dot{x}(t)) = 0.5((1 + \tanh(\dot{x}(t))\alpha_1 + (1 - \tanh(\dot{x}(t))\alpha_2) = \frac{\alpha_1 e^{2\dot{x}(t)} + \alpha_2}{e^{2\dot{x}(t)} + 1}$

In Eqs. (8) and (9), $\alpha_x(\dot{x}(t)) > 0$ is a continuous function that allows for a smooth transition from the loading and unloading phases and vice versa; $\alpha_1 > 0$, $\alpha_2 > 0$, A, ϑ, δ are parameters that control the shapes of hysteresis loops in loading and unloading phases, displacement output $\Phi_{Asym}(x)(t) = x_{out}(t)$, and displacement input $x(t) = x_{in}(t)$.

The parameters are optimized based upon the minimization of the error of $x_{out}(t)$ from the measured output using Genetic Algorithm (GA) as shown in the upper panel of Fig. 3; this results in $\alpha_1 = 0.8972$, $\alpha_1 = 0.9487$, $A = -0.8745$, $\vartheta = 5.034$, $\delta = 0.1452$. The predicted backlash hysteresis loop is shown in Fig. 6. As shown in the figure, the backlash hysteresis curves are asymmetric for the loading and unloading phases. In addition, there are different slopes for both phases.

The mean square error (MSE) for the proposed model and the generalized asymmetric Bouc–Wen model given in Section 3.2 in this case is about 7.84×10^{-3} and 1.89×10^{-3} respectively. The same error for the symmetric Bouc–Wen model given by Section 3.1 is about 1.34×10^{-2}. Unlike the models mentioned in Sections 3.1 and 3.2, the proposed model only requires five (5)

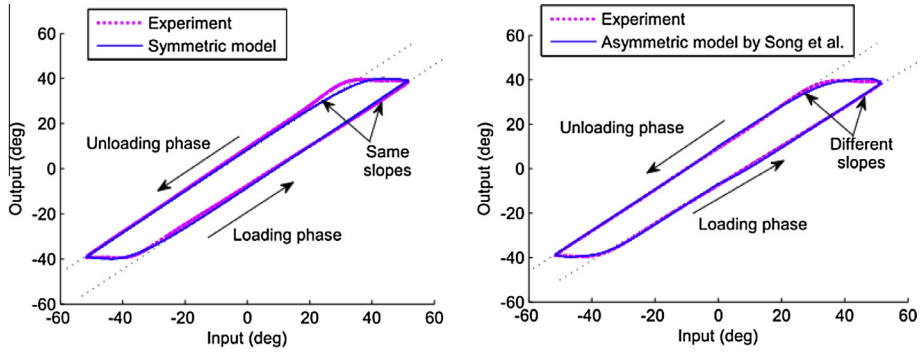

Fig. 5. Backlash hysteresis nonlinearity predicted by symmetric (left) and generalized asymmetric (right) Bouc–Wen model of hysteresis. The unit for displacement is expressed in degree.

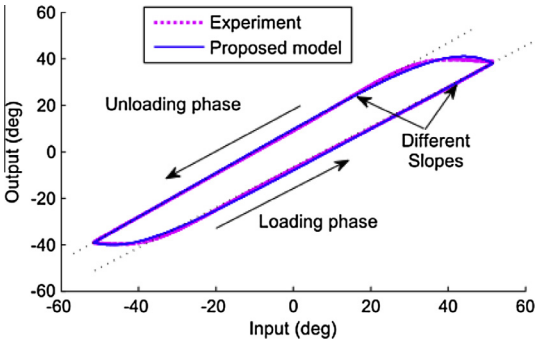

Fig. 6. Backlash hysteresis nonlinearity predicted by the proposed model. The unit for displacement is expressed in degree.

parameters without sacrificing its accuracy in both phases. The comparison for models is given in Table 1.

4. Parameter identification method for the proposed model

Genetic Algorithm (GA) is a global search method based on natural selection and genetics including operators of crossover, mutation, reproduction [31,32]. This method employs natural evolution to move from one population of "chromosomes" to a new population where unfit components are eliminated. The GA generates the next generations using operators and evaluates the future chromosomes based on a fitness function. This fitness function will be used as a stop condition. For identification of the proposed model parameters, the optimization is used to determine a set of five (5) parameters given by Eqs. (7)–(9). In order to match the model output with the experimental results, the fitness function given by Eq. (10) is used. The goal is to minimize this fitness function to get the best result of model parameters under relevant constraints.

$$Min_{parameters} f(x) = \frac{1}{N}\sum_{i=1}^{N}\left(x_{out}(i) - \widehat{\Phi}_{Asym}(i)\right)^2 \quad (10)$$

where i is sampling index and N is total number of samples from experimental results, x_{out} is actual displacement at distal end of the tendon-sheath mechanism. $\widehat{\Phi}$ is the estimated backlash hysteresis nonlinearity at distal end of the tendon sheath mechanism. The fitness function $Min_{parameters} f(x)$ is defined as the mean square error between the proposed model and actual experimental data.

The GA is used to generate an initial guess of model parameters. The Nelder–Mead Simplex method is subsequently applied to refine the identified results. It is a direct search method that can be utilized to predict the best solution of the model parameters. The optimisation process is using MATLAB Identification Toolbox and the *fminsearch* command. The model parameters can be identified if the input signal $x_{in}(t)$ and output signal $x_{out}(t)$ are known. The relative velocity $\dot{x}_{in}(t)$ is obtained using numerical differentiation of the measured displacement input $x_{in}(t)$. The data in the identification process are filtered using zero-phase digital filtering with *filtfilt* command in MATLAB.

5. Controller design for the tendon-sheath mechanism based on the proposed model

A feedforward control scheme based on the inverse multiplicative method is proposed and implemented to improve the tracking performance of the distal end. This method is used in many applications of piezoelectric actuations because it does not require any complex inversions of backlash hysteresis model and allows for easy implementations [21–23]. In addition, this method does not require adaptive nonlinear control algorithms to guarantee the controller continuity as in approaches [22,33–37]. Due to the restriction on size and sterilization requirement, the slave side cannot be equipped with sensors to measure the backlash hysteresis displacement during the operations. In such case, the backlash hysteresis observers based on the proposed model given by Eqs. (7)–(9) are used to estimate the displacement output of the tendon-sheath system. The proposed controller based on these estimated values is able to minimize the displacement errors between the output, $x_{out}(t)$, and the reference input, $x_r(t)$.

Table 1
Comparison for models.

Model	Advantages	Disadvantages
Symmetric Bouc–Wen model	Simple with six parameters in model, independent curve angles and configuration	Cannot capture asymmetric slopes for loading and unloading phases, an approximation of backlash hysteresis model
Generalized asymmetric Bouc–Wen model	Can capture asymmetric slopes for both phases, independent curve angles and configuration	Too many parameters in model structure (ten parameters to be identified), an approximation of asymmetric backlash hysteresis model
Proposed model	Simple with five parameters in model structure, capture well asymmetric loops for both phase, independent curve angles and configuration	An approximation of asymmetric backlash hysteresis model

5.1. Feedforward controller design and compensation

Consider a reference signal of displacement, $x_r(t)$, and the backlash hysteresis displacement at the distal end $\Phi_{Asym}(t) = x_{out}(t)$ given by Eqs. (8) and (9). With a new control input $x_{FF}(t)$ at the proximal end, a feedforward compensator based on the estimated backlash hysteresis $\hat{\zeta}(t)$ and smooth function $\alpha_x(\dot{x}_r(t))$ can be designed as follows:

$$x_{FF}(t) = \frac{1}{\alpha_x(\dot{x}_r(t))}(x_r(t) - \hat{\zeta}(t)) \tag{11}$$

where $\hat{\zeta}(t)$ is estimated values of $\zeta(t)$ and $\alpha_x(\dot{x}_r(t))$ is a smooth function given in Section 3.4.

The estimated values and the smooth function are shown in Figs. 7 and 8, and are given by:

$$\dot{\hat{\zeta}}(t) = A\dot{x}_r(t) - \vartheta|\dot{x}_r(t)|\hat{\zeta}(t) + \delta|\dot{x}_r(t)| \tag{12}$$

$$\alpha_x(\dot{x}_r(t)) = \frac{\alpha_1 e^{2\dot{x}_r(t)} + \alpha_2}{e^{2\dot{x}_r(t)} + 1} \tag{13}$$

By substituting Eq. (11) into Eq. (9), the relationship between the output displacement $x_{out}(t)$ and the reference displacement $x_r(t)$ is given by:

$$\begin{aligned} x_{out}(t) &= \alpha_x(\dot{x}_r(t))\frac{1}{\alpha_x(\dot{x}_r(t))}(x_r(t) - \hat{\zeta}(t)) + \zeta(t) \\ &= x_r(t) + \zeta(t) - \hat{\zeta}(t) \end{aligned} \tag{14}$$

The block diagrams for the estimated variables $\hat{\zeta}(t)$ and smooth function $\alpha_x(\dot{x}_r(t))$ are shown in Figs. 7 and 8, respectively. If the estimated values $\hat{\zeta}(t) = \zeta(t)$ then the errors between the reference input and output displacement will be eliminated. This means that the output displacement $x_{out}(t)$ will follow the input reference $x_r(t)$. For the DC-motor loop, a saturation function is appended to constraint the output signals of controller to between 0 and 24 VDC, which is the voltage range applied to the motor. The left panel of Fig. 9 shows the block diagram of the system without a feedforward loop, while right panel shows that with a feedforward compensation scheme given by Eqs. (11)–(13). It is shown that the accuracy of the control is based on the performance of hysteresis observers given by Eq. (12).

5.2. Implementation of real-time compensation and discussions

This section discusses the identification results for the proposed model and the real-time implementation of the proposed control scheme. The proposed schemes are experimentally implemented to validate their effects on enhancing the position-tracking performances of the tendon-sheath mechanism.

5.2.1. Identification results and comparison

In the real-time implementation, any input excitations might be applied to the reference displacement input, $x_r(t)$. As discussed in Section 3, the parameters of the proposed model can be identified using GA and Nelder–Mead Simplex method. The identified parameters for a sinusoidal signal with frequency of 0.2 Hz and amplitude of 56° as shown in the upper panel of Fig. 3 are performed with $\alpha_1 = 0.8972$, $\alpha_2 = 0.9487$, $A = -0.8745$, $\vartheta = 5.034$, $\delta = 0.14522$. The backlash hysteresis curves of the proposed model and experimental results are shown in Fig. 10: the left panel presents the time history of output and the corresponding error, while the right panel shows the functional relationship between the input and output from both the experiment and proposed model. It is noted that these model parameters can also be used for multi-periodic inputs consisting of two signals as shown in the middle panel of Fig. 3. The results are shown in Fig. 11.

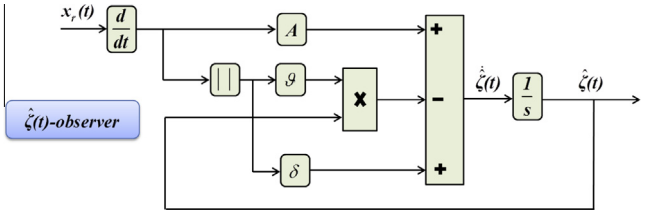

Fig. 7. Block diagram of estimated backlash hysteresis $\hat{\zeta}(t)$ given by Eq. (12).

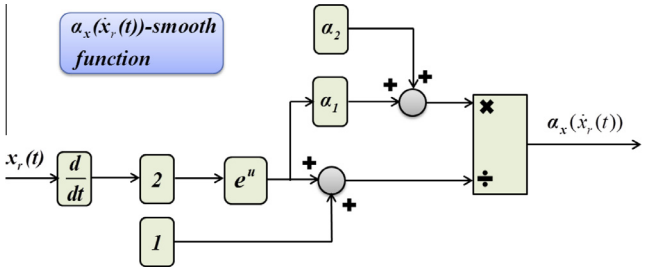

Fig. 8. Block diagram of smooth function $\alpha_x(\dot{x}_r(t))$ given by Eq. (13).

An input signal comprising of a sequence of non-harmonics shown in the lower panel of Fig. 3 is used next. The model parameters for this case are similar to those at the above cases. Fig. 12 shows the comparison between identification results and experimental data. The left panel presents the time history of the real experiment and the predicted model given by Eqs. (7)–(9). The identification error is also given in this panel. The right panel is represented for the relation between the displacement input and output signal. From these, it can be concluded that there is a good agreement between the proposed model and the real experimental data for periodic and non-periodic input signals applied to the tendon-sheath system.

5.2.2. Position tracking performance of the proposed control scheme

To validate the model applied in the control scheme in real-time implementations, different excitation signals are used. Fig. 13(a) shows the time history of a reference sinusoidal signal, $x_r(t)$, with 55° of amplitude and frequency of 0.2 Hz as shown in Section 5.2.1. The time history of measured output signal $x_{out}(t)$ based on the feedforward compensation and the corresponding errors are shown in this figure.

The effectiveness of the feedforward control scheme is illustrated in Fig. 13(b) for a single sinusoidal input signal. It can be observed that without feedforward compensation, the error between the reference input $x_r(t)$ (see the left panel of Fig. 9) and the measured output $x_{out}(t)$ (at distal end) is rather high (27° peak-to-peak). When a feedforward scheme is applied (see the right panel of Fig. 9), this error is significantly reduced (8° peak-to-peak). The control input x_{FF} is shown in Fig. 13(c) and the relation between input and output, before and after compensation is presented in Fig. 13(d).

Fig. 14 illustrates the real-time compensation of a multi-periodic motion with feedforward control. Utilizing the observer given in Eq. (12) and the smooth function in Eq. (13), together with the model parameters given in Section 5.2.1, the tracking performance for the system is improved, where the peak-to-peak error is reduced from 27° to 8.5° after compensation with the feedforward loop (Fig. 14(b)). The time history of the control input x_{FF} and the relation between input and output are also presented in Fig. 14(c) and (d), respectively.

In the case of a non-harmonic input sequence, the effectiveness of the asymmetric backlash hysteresis model and its observer are

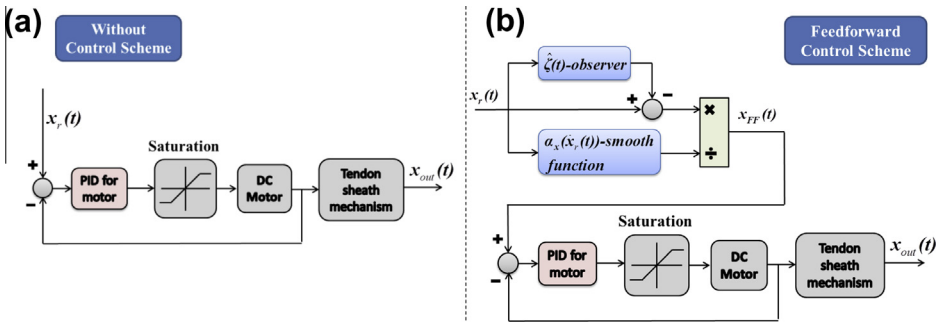

Fig. 9. Block diagram of the system; (a) without feedforward; and (b) with feedforward compensation scheme for tendon-sheath mechanism.

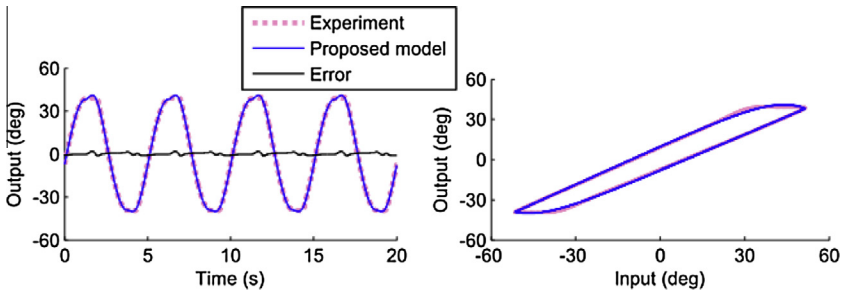

Fig. 10. Identified results for input signal of 0.2 Hz in frequency. The unit for displacement is expressed in degree.

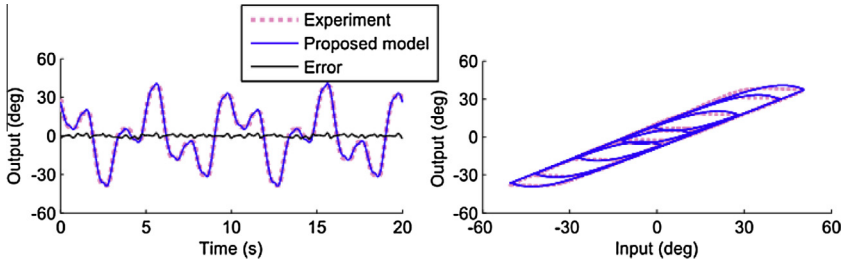

Fig. 11. Identified results for multi-periodic input combined by two signals of 0.2 Hz and 0.5 Hz in frequency. The unit for displacement is expressed in degree.

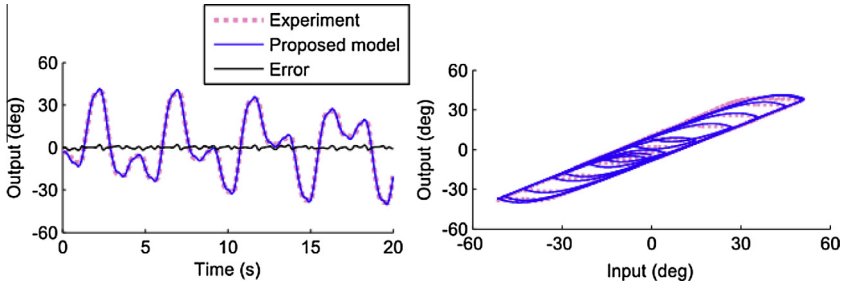

Fig. 12. Identified results for a non-harmonic sequence of input signal with frequencies of 0.25 Hz and $0.25\sqrt{3}$ Hz. The unit for displacement is expressed in degree.

demonstrated in terms of the tracking performances. As shown in Fig. 15, the maximum peak-to-peak error before compensation is around 28° and after applying the compensation scheme, the error is reduced to 9.2°. From these results, it is shown that the proposed schemes are not only efficient for periodic motions but also well suited for non-periodic motions.

6. Discussion

In the previous sections, the simulations and real-time implementations of the proposed model and control schemes were presented for the tendon sheath systems. The controller scheme does not need any complex inverse models, which will require us to re-evaluate the parameters of the inverse model and to use a nonlinear control algorithm. In our approach, the compensator is directly developed based on the proposed model.

The control scheme based on the proposed model gives a good tracking performance. It has been shown that the approach works well not only with periodic and multi-periodic motions but also for a non-harmonic sequence of motion. This feature is very important for surgical robots because most of the surgeons' motions are typically non-harmonic.

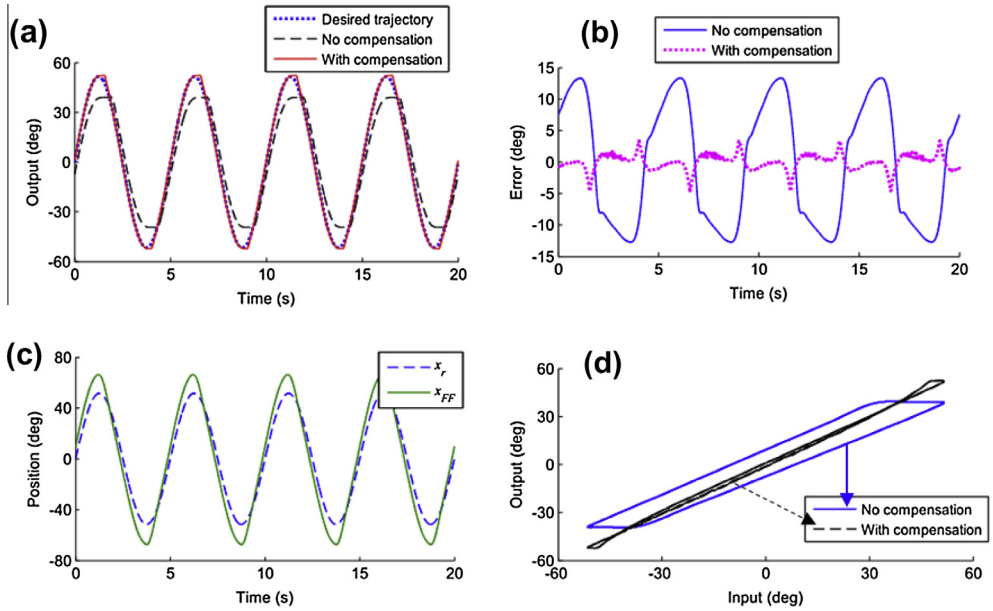

Fig. 13. (a) The time histories of single frequency reference and measured output signals; (b) error results; (c) the time history of control input and reference signal; and (d) input vs. output. The unit for displacement is expressed in degree.

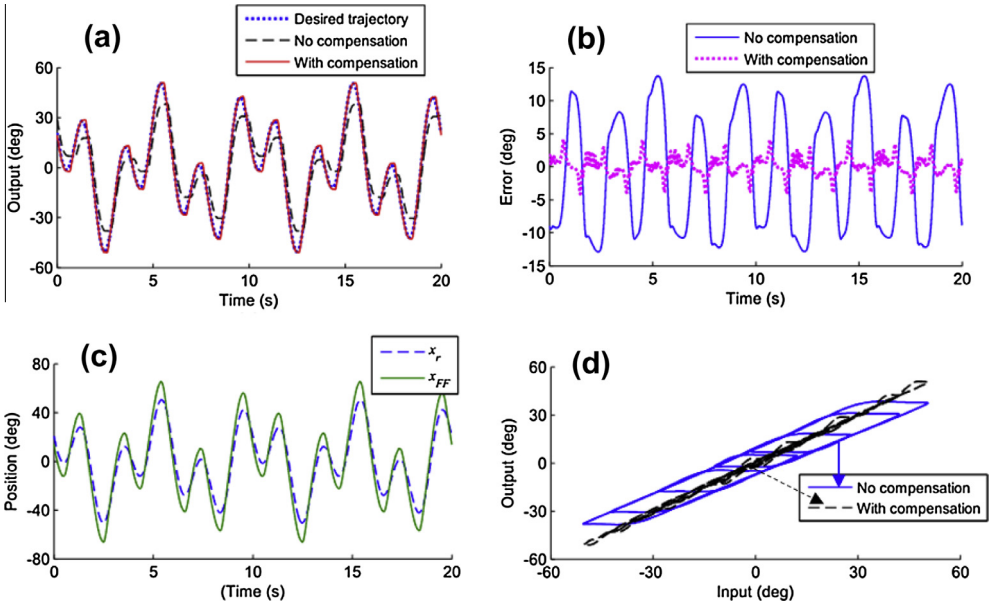

Fig. 14. (a) The time histories of periodic reference and measured output signals; (b) error results; (c) the time history of control input and reference signal; and (d) input vs. output. The unit for displacement is expressed in degree.

Based on the authors' knowledge, current control approaches in the literature only demonstrated results for a periodic motion and the model parameters depend on the tendon-sheath configuration. The results demonstrated that the controller based on the proposed model is able to enhance the tracking performances of the tendon-sheath in endoscopic systems for any configurations. This comes from the fact that our proposed model does not depend on the sheath curve angles.

However, it has to be highlighted that the proposed model is developed based on several assumptions such as the tension of the tendon is always maintained by an initial pretension in order to avoid the slack of the tendon and the accumulated curve angles of the sheath should not change during the experiment. Nonetheless, the proposed model structure is independent of the tendon-sheath configuration as long as the accumulated curve angles remain, which is not the case on the current approaches found in literatures [1,5–8,10–13].

Due to size constraint and sterilization problem, sensors cannot be mounted at the tool tips of robotic arms. Therefore, necessary feedbacks such as position and force for the tendon sheath system are not available. In such cases, only a feedforward control scheme is applicable to compensate for the nonlinearities. Because the accuracy of compensation depends on the model parameters and observers, there still exist slight errors in the tracking result. For some surgical devices such as the Laproteck robot arm or the MRI compatible system [14,38,39], information at the tool tips

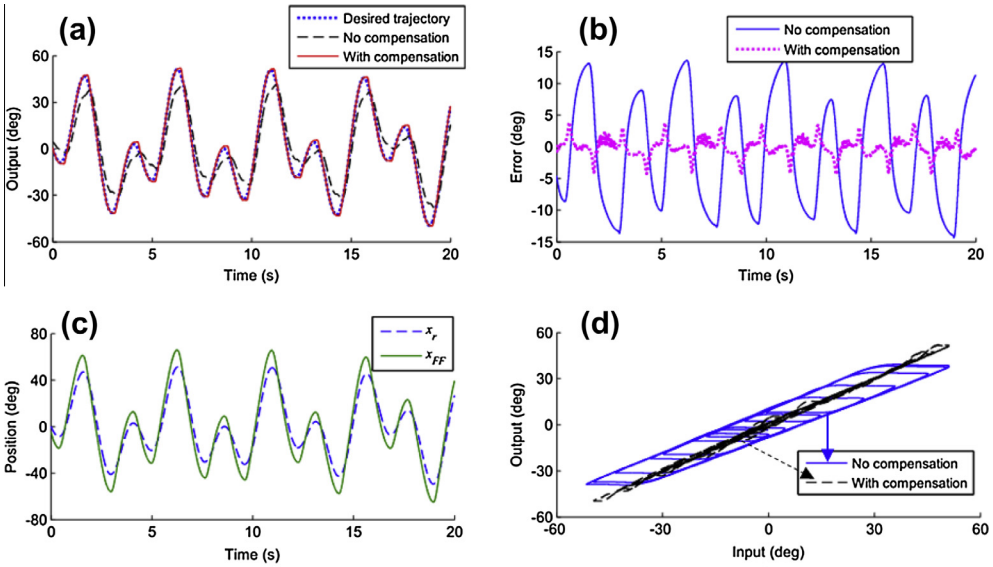

Fig. 15. (a) The time histories of non-periodic reference and measured output signals; (b) error results; (c) the time history of control input and reference signal; and (d) input vs. output. The unit for displacement is expressed in degree.

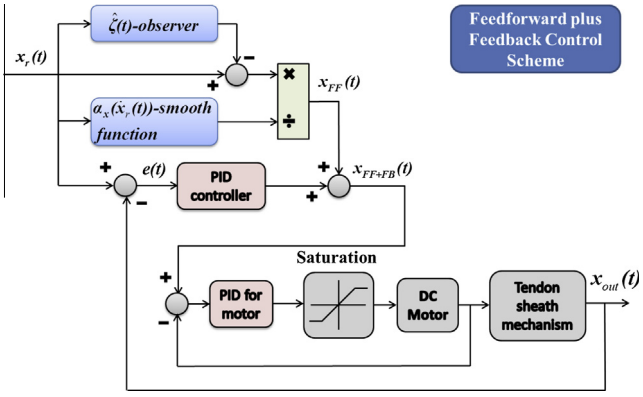

Fig. 16. Block diagram for controller with feedforward and feedback combination.

may be available for feedback. In such cases, a combination between the feedforward-based the proposed model and feedback control scheme is beneficial to enhance the tracking performances and reduce the errors [21,40]. The structure of this scheme is illustrated by Fig. 16.

According to Fig. 16, the feedforward control scheme given by Eqs. (11)–(14) are combined with a PID feedback controller in the following equation:

$$x_{FF+FB}(t) = x_{FF}(t) + K_P e(t) + K_I \int e(t)dt + K_D \frac{de(t)}{dt} \tag{15}$$

where $e(t) = x_r(t) - x_{out}(t)$ is the tracking error with $x_r(t)$ as the reference input signal, $x_{out}(t)$ the measured output at distal end of the tendon-sheath system, K_P, K_I, K_D as the control parameter of proportional gain, integral gain, and derivative gain, respectively.

To show the tracking performance between two proposed schemes, a single periodic motion is considered, where the model parameters are $\alpha_1 = 0.9477$, $\alpha_2 = 0.9333$, $A = -0.8130$, $\vartheta = 4.3820$, $\delta = -0.0570$. The PID controller is applied with gains of $P = 1.5$, $I = 2$, $D = 0$.

Fig. 17 presents the real-time compensation results for the tendon-sheath mechanism under two control schemes. By introducing a combination of feedforward and feedback loop, the tracking error is reduced to 5.8° from 8° when we only utilize feedforward loop as shown in Fig. 17.

From these results, it can be concluded that a feedforward plus feedback control scheme can achieve better tracking performances than a single feedforward scheme. However, the combined scheme needs output feedback at the tool tips, which can result in increasing the DoFs in the slave, and consideration of safety issues in surgical applications.

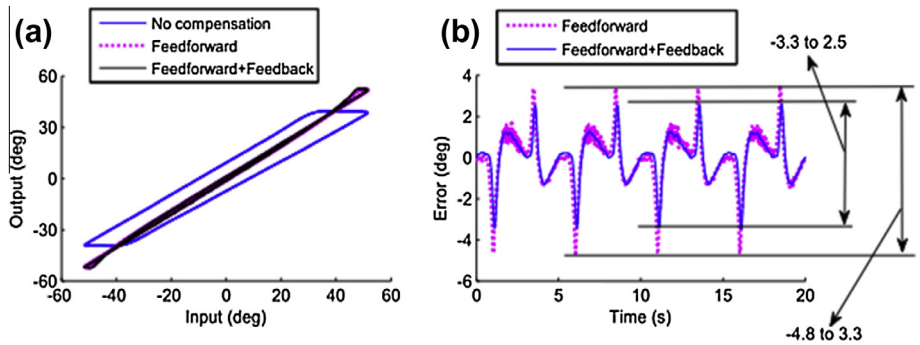

Fig. 17. Comparison results (the unit for displacement is expressed in degree); (a) position input vs. position output and (b) error results.

7. Conclusion

The advantages of being light weight, safe, small size, and flexible, make the tendon-sheath mechanism a suitable mode of transmission in flexible endoscopic systems. However, nonlinear phenomena such as backlash hysteresis in this mechanism pose a big challenge in current surgical applications. In this paper, we have proposed schemes including modelling, identification, and control to enhance the tracking performances for the tendon-sheath mechanism in flexible endoscopic robots.

The proposed model has a reduced number of model parameters compared to the original asymmetric Bouc–Wen model and enhances the tracking performances of the tendon-sheath. In comparison with current approaches in the literature, the proposed model is better able to track backlash hysteresis nonlinearities in the tendon-sheath mechanism with less effort in computation and in the identification processes. The application of the proposed model for feedforward control scheme has been demonstrated in this paper. The control structure is simple to use because it uses the proposed model directly in the controller design.

As observed from the experimental results, the backlash hysteresis nonlinearity is independent of the tendon-sheath configuration as long as the accumulated curve angles are maintained. Therefore, the proposed model allows for arbitrarily changes of the tendon-sheath configuration. It means that the model is good for any tendon-sheath configurations with a fixed accumulated curve angle.

In order to reduce the tracking error further, a combination of feedforward and feedback control scheme has also been demonstrated assuming that output feedback is available. However, under some constraints, in the absence of the output feedback, a feedforward control scheme is more suitable.

Future activities will be conducted by developing models and control schemes for a pair of tendon-sheath systems to adapt to any configuration. A nonlinear adaptive control schemes will be developed to take into account disturbances as well as flexible changes of configuration during real-time implementation. A higher two DOFs will be considered in the next phase of the research as well as in vivo experimental works will be undertaken.

References

[1] Phee SJ, Low SC, Huynh VA, Kencana AP, Sun ZL, Yang K. Master and slave transluminal endoscopic robot (MASTER) for natural Orifice Transluminal Endoscopic Surgery (NOTES). In: Annual international conference of the IEEE engineering in medicine and biology society (MBC); 2009. p. 1192–5.

[2] Bardou B, Nageotte F, Zanne P, de Mathelin M. Improvements in the control of a flexible endoscopic system, In: IEEE international conference on robotics and automation (ICRA); 2012. p. 3725–32.

[3] Abbott DJ, Becke C, Rothstein RI, Peine WJ. Design of an endoluminal NOTES robotic system. In: IEEE/RSJ international conference on intelligent robots and systems, IROS; 2007. p. 410–6.

[4] Dachs Ii GW, Peine WJ. A novel surgical robot design: Minimizing the operating envelope within the sterile field. In: 28th Annual international conference of the ieee engineering in medicine and biology society, EMBS'06. New York (NY), United States: Institute of Electrical and Electronics Engineers Inc., August 30, 2006–September 3, 2006. p. 1505–8.

[5] Kaneko M, Yamashita T, Tanie K. Basic considerations on transmission characteristics for tendon drive robots. In: Fifth international conference on advanced robotics, 'Robots in Unstructured Environments' (ICAR), vol. 821; 1991.p. 827–32.

[6] Kaneko M, Paetsch W, Tolle H. Input-dependent stability of joint torque control of tendon-driven robot hands. IEEE Trans Indust Electron 1992;39:96–104.

[7] Palli G, Melchiorri C. Model and control of tendon-sheath transmission systems. In: Proceedings of IEEE international conference on robotics and automation (ICRA); 2006. p. 988–93.

[8] Palli G, Melchiorri C. Optimal control of tendon-sheath transmission systems. In: 8th International IFAC symposium on robot control, SYROCO 2006. Bologna, Italy, September 6, 2006–September 8, 2006.

[9] Dahl PR. A solid friction model. El Segundo (CA): Aerospace Corp.; 1968. p. 31.

[10] Tian F, Wang X. The design of a tendon-sheath-driven robot. In: 15th International conference on mechatronics and machine vision in practice (M2VIP); 2008. p. 280–84.

[11] Low Soon C, Phee Soo J, Valdastri P, Menciassi A, Dario P. Tendon sheath analysis for estimation of distal end force and elongation. IEEE/ASME international conference on advanced intelligent mechatronics (AIM); 2009. p. 332–7.

[12] Agrawal V, Peine WJ, Yao B. Modeling of a closed loop cable-conduit transmission system. In: IEEE international conference on robotics and automation (ICRA); 2008. p. 3407–12.

[13] Agrawal V, Peine WJ, Yao B. Modeling of transmission characteristics across a cable-conduit system. IEEE Trans Robot 2010;26:914–24.

[14] Agrawal V, Peine WJ, Yao B, Choi S. Control of cable actuated devices using smooth backlash inverse. In: IEEE international conference on robotics and automation (ICRA); 2010. p. 1074–9.

[15] Agrawal V, Peine WJ, Yao B. Dual loop control of cable-conduit actuated devices. In: American control conference (ACC); 2012. p. 2621–6.

[16] Kesner SB, Howe RD. Design and control of motion compensation cardiac catheters. In: IEEE international conference on robotics and automation (ICRA); 2010. p. 1059–65.

[17] Kesner SB, Howe RD. Position control of motion compensation cardiac catheters. IEEE Trans Robot 2011;27:1045–55.

[18] Zglimbea R, Finca V, Greaban E, Constantin M. Identification of systems with friction via distributions using the modified friction LuGre model. In: ICS'09 proceedings of the 13th WSEAS international conference on systems; 2009. p. 579–84.

[19] Hassani V, Tjahjowidodo T. Structural response investigation of a triangular-based piezoelectric drive mechanism to hysteresis effect of the piezoelectric actuator. Mech Syst Signal Process 2013;36:210–23.

[20] Ikhouane F, Rodellar J. Systems with hysteresis: analysis: identification and control using the Bouc–Wen model. Hoboken: John Wiley & Sons, Ltd.; 2007.

[21] Lin C-J, Lin P-T. Tracking control of a biaxial piezo-actuated positioning stage using generalized Duhem model. Comput Math Appl 2012;64:766–87.

[22] Rakotondrabe M. Bouc–Wen modeling and inverse multiplicative structure to compensate hysteresis nonlinearity in piezoelectric actuators. IEEE Trans Autom Sci Eng 2011;8:428–31.

[23] Wang DH, Zhu W, Yang Q. Linearization of stack piezoelectric ceramic actuators based on Bouc–Wen model. J Intell Mater Syst Struct 2011;22:401–13.

[24] Tao G, Kokotovic PV. Adaptive control of systems with backlash. Automatica 1993;29:323–35.

[25] Biggers K, Jacobsen SC, Gerpheide G. Low level control of the Utah/M.I.T. dextrous hand. In: Proceedings of IEEE international conference on robotics and automation; 1986. p. 61–6.

[26] Su CY, Stepanenko Y, Svoboda J, Leung TP. Robust adaptive control of a class of nonlinear systems with unknown backlash-like hysteresis. IEEE Trans Autom Control 2000;45:2427–32.

[27] Yu Y, Naganathan N, Dukkipati R. Preisach modeling of hysteresis for piezoceramic actuator system. Mech Mach Theory 2002;37:49–59.

[28] Yang M-J, Gu G-Y, Zhu L-M. Parameter identification of the generalized Prandtl–Ishlinskii model for piezoelectric actuators using modified particle swarm optimization. Sens Actuat A: Phys 2013;189:254–65.

[29] Ikhouane F, Hurtado J, Rodellar J. Variation of the hysteresis loop with the Bouc–Wen model parameters. Nonlin Dynam 2007;48:361–80.

[30] Song J, Der Kiureghian A. Generalized Bouc–Wen model for highly asymmetric hysteresis. J Eng Mech 2006;132:610–8.

[31] Mitchell M. Introduction to genetic algorithms. MIT Press; 1996.

[32] Tjahjowidodo T, Al-Bender F, Van Brussel H, Symens W. Friction characterization and compensation in electro-mechanical systems. J Sound Vib 2007;308:632–46.

[33] Zhu G, Lei H. Adaptive backstepping control of a class of unknown backlash-like hysteresis nonlinear systems. In: 8th International conference on electronic measurement and instruments, ICEMI '07; 2007. p. 3-776–3-781.

[34] Han KH, Koh GO, Sung J, Kim BS. An adaptive control approach for improving control systems with unknown backlash. Int J Aeronaut Space Sci 2011;12:360–4.

[35] Ikhouane F, Mañosa V, Rodellar J. Adaptive control of a hysteretic structural system. Automatica 2005;41:225–31.

[36] Zhou J, Wen C, Zhang Y. Adaptive output control of nonlinear systems with uncertain dead-zone nonlinearity. IEEE Trans Autom Control 2006;51:504–11.

[37] Zhou J, Wen C, Li T. Adaptive output feedback control of uncertain nonlinear systems with hysteresis nonlinearity. IEEE Trans Autom Control 2012;57:2627–33.

[38] Melchiorri C, Vassura G. Mechanical and control features of the University of Bologna hand version 2. In: Proceedings of the IEEE/RSJ international conference on intelligent robots and systems; 1992. p. 187–93.

[39] Zion Tsz Ho T, Elhawary H, Zivanovic A, Rea M, Paley M, Bydder G, et al. A 3-DOF MR-compatible device for magic angle related in vivo experiments. IEEE/ASME Trans Mechatron 2008;13:316–24.

[40] Minh TV, Tjahjowidodo T, Ramon H, Van Brussel H. Cascade position control of a single pneumatic artificial muscle-mass system with hysteresis compensation. Mechatronics 2010;20:402–14.